Parity-odd multipoles, magnetic charges and chirality in haematite (α−Fe$_2$O$_3$)

S. W. Lovesey

ISIS Facility & Diamond Light Source Ltd, Oxfordshire OX11 0QX, United Kingdom

A. Rodríguez-Fernández and J. A. Blanco

Departamento de Física, Universidad de Oviedo, E–33007 Oviedo, Spain

(Dated: December 2, 2013)

Collinear and canted magnetic motifs in haematite were investigated by Kokubun *et al.* [Phys. Rev. B 78, 115112(2008)]. using x-ray Bragg diffraction magnified at the iron K-edge, and analyses of observations led to various potentially interesting conclusions. We demonstrate that the reported analyses for both non-resonant and resonant magnetic diffraction at low energies near the absorption K–edge are not appropriate. In its place, we apply a radically different formulation, thoroughly tried and tested, that incorporates all magnetic contributions to resonant x-ray diffraction allowed by the established chemical and magnetic structures. Essential to a correct formulation of diffraction by a magnetic crystal with resonant ions at sites that are not centres of inversion symmetry are parity-odd atomic multipoles, time-even (polar) and time-odd (magneto-electric), that arise from enhancement by the electric-dipole (E1) - electric-quadrupole (E2) event. Analyses of azimuthal-angle scans on two space-group forbidden reflections, hexagonal $(0, 0, 3)_h$ and $(0, 0, 9)_h$, collected by Kokubun *et al.* [Phys. Rev. B 78, 115112(2008)] above and below the Morin temperature ($T_M = 250\,K$), allow us to obtain good estimates of contributing polar and magneto-electric multipoles, including the iron anapole. We show, beyond reasonable doubt, that available data are inconsistent with parity-even events only (E1-E1 and E2-E2). For future experiments, we show that chiral states of haematite couple to circular polarization and differentiate E1-E2 and E2-E2 events, while the collinear motif supports magnetic charges.

PACS numbers: 78.70.Ck, 78.20.Ek, 75.50.Ee, 75.47.Lx,

I. INTRODUCTION

Enigmas about ichor-like haematite (α–Fe_2O_3) and famed lodestone, both real and concocted, have been worried and written about from the time of Greek texts in 315 B.C., to William Gilbert of Colchester, the father of magnetism, in the 16th. C., to Dzyaloshinsky in 1958 who gave a phenomenological theory of weak ferromagnetism. Haematite is the iron sesquioxide that crystallizes into the corundum structure (centro-symmetric space-group $\sharp$167, $R\bar{3}c$) in which ferric (Fe^{3+}, $3d^5$) ions occupy sites 4(c) on the trigonal c-axis that are not centres of inversion symmetry. For an extensive review of the history and properties of haematite see, for example, Morrish[1] and Catti et al.[2]

At room temperature, the motif of magnetic moments is canted antiferromagnetism with moments in a (basal) plane normal to the c-axis. Weak ferromagnetism parallel to a diad axis of rotation symmetry, normal to a mirror plane of symmetry that contains the c-axis, is created by a Dzyaloshinsky-Moriya antisymetric interaction $\mathbf{D} \cdot (\mathbf{S_1} \times \mathbf{S_2})$ between spins $\mathbf{S_1}$ and $\mathbf{S_2}$ and the vector $\mathbf{D}$ is parallel to the c-axis, Dzyaloshinsky,[3] Moriya.[4] The Morin temperature 250 K, at which moments rotate out of the the basal plane to the c-axis, may be determined from the temperature dependence of magnetic Bragg peaks observed by neutron diffraction. Rotation of the moments takes place in a range of 10 K in pure crystals but the interval can be much larger, $\approx$ 150 K, in mixed materials.[5] Ultimately, moments align with the c-axis and create a fully compensating, collinear antiferromagnet with an iron magnetic moment = 4.9 μ_B at 77 K. We follow Dzyaloshinsky[3] and label collinear (low-temperature phase) and canted (room-temperature phase) antiferromagnetism as phases I and II, respectively, see figure 1. In phase I haematite is not magneto-electric unlike eskolaite (Cr_2O_3), which also possesses the corundum structure and collinear antiferromagnetism.
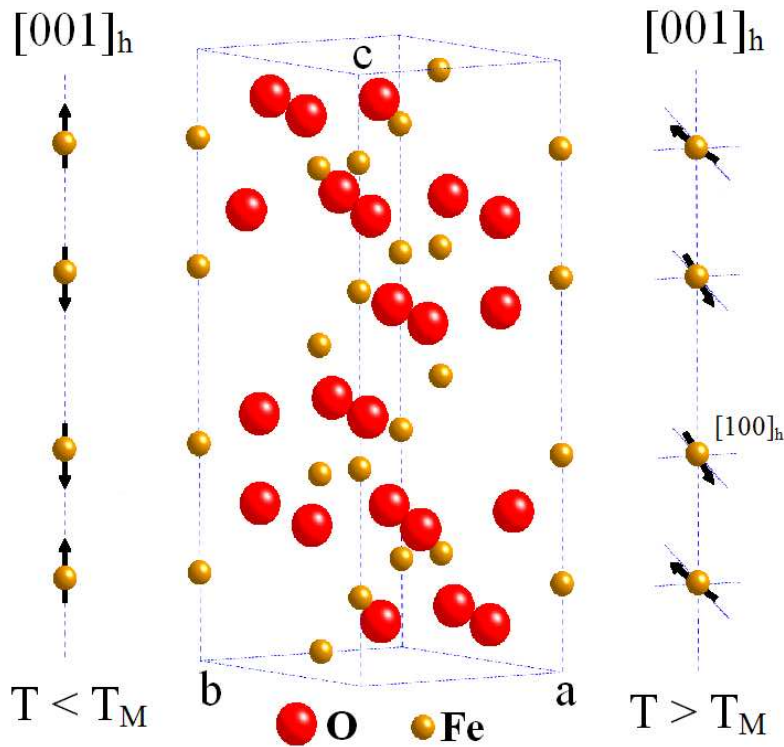

FIG. 1. Magnetic and chemical structure of haematite, space group $R\bar{3}c$. The red and the yellow dots represent oxygen and iron sites, respectively. The left line denotes the magnetic motif along the c-axis below the Morin temperature (Phase I). The right line denotes the motif above the Morin temperature, where iron moments are contained in the a-b plane (Phase II).

Finkelstein et al.[6] and Kokubun et al.[7] studied haematite by x-ray Bragg diffraction, with Bragg intensities enhanced by tuning the energy of the primary x-rays to the iron K-absorption edge. In these experiments, attention is given to Bragg reflections that are forbidden by extinction rules for the space-group. Often called Templeton and Templeton reflections,[8] the reflections in question are relatively weak and arise from angular anisotropy of valence states that accept the photo-ejected electron. Following rotation of the crystal about a Bragg wave-vector aligned with the c-axis, Finkelstein et al.[6] observed a near six-fold periodicity of the intensity that is traced to a triad axis of rotation symmetry that passes through sites occupied by resonant, ferric ions. In general by measuring intensities, collected at space-forbidden reflections, we can obtain information of high-order multipoles existing in the materials such as magnetic

charge (or magnetic monopole),[9] electric dipole,[10] anapole,[11,12] quadropole,[13] octupole[14,15] and hexadecapole.[16,17] Therefore, these weak reflections are extremely sensitive to charge, orbital and spin electron degrees of freedom and haematite is no exception.[18]

We apply an atomic theory of resonant Bragg diffraction formulated for the corundum structure,[19] to data gathered by Kokubun et $al.$[7] at forbidden reflections $(0,0,l)_h$ with $l = 3(2n+1)$ and infer from available data relative values of atomic multipoles of the resonant ion. A successful story emerges with scattering represented by a mixture of parity-even and parity-odd (even or odd with respect to the inversion of space) multipoles at sites in the structure occupied by resonant iron ions, which are not centres of inversion symmetry. Parity-odd multipoles arise in a resonant event using the electric dipole (E1) and electric quadrupole (E2) - corresponding multipoles are labelled polar (time-even) or magneto-electric (time-odd) - while parity-even multipoles arise from E1-E1 and E2-E2 events. A chiral state of haematite is demonstrated by a predicted coupling of resonant intensity to circular polarization (helicity) in the primary beam, and the effect also differentiates between E1-E2 and E2-E2 events. The two parity-odd multipoles of rank zero correspond to chirality and magnetic charge[20,21] and both pseudo-scalar monopoles are present in the electric dipole-magnetic dipole (E1-M1) amplitude for resonant scattering by haematite in phase I.

Our communication is arranged as follows. Section 2 contains essential information and definitions. Unit-cell structure factors for Bragg diffraction enhanced by E1-E1, E1-E2 and E2-E2 listed in an Appendix are exploited in Sections 3 and 4, which report the successful analysis of Bragg diffraction data gathered on haematite at room temperature and 150 K, well below the Morin transition. Thereafter, in Section 5, there are simulations of resonant intensity induced by circular polarization in the primary x-ray beam which signals existence of a chiral state. Section 6 addresses magnetic charge found in the E1-M1 structure factor, and not visible in a dichroic signal. A discussion of findings in Section 7 concludes the communication.

II. BASICS

There are four contributions to the amplitude of photons scattered by electrons calculated in the first level of approximation in the small quantity (E/mc^2), where E is the energy of the primary photon, namely, Thomson scattering, spin scattering and two contributions with virtual intermediate states, one of which may become large when E coincides with an atomic resonance. Of particular interest with magnetic samples is a celebrated reduction of the amplitude, derived by de Bergevin and Brunel,[22] which occurs at large E. In this limit, all three contributions excluding Thomson scattering add to give so-called magnetic, non-resonant scattering made up simply of spin and orbital magnetic moments. De Bergevin and Brunel's result is not valid at low energies, and certainly not below an atomic resonance, as is at once obvious from steps in its derivation.[23]

In an analysis of x-ray Bragg diffraction data for haematite collected at space-group forbidden reflections we use the spin and resonant contributions to the scattering amplitude. The spin contribution $G^s = i(E/mc^2)(\mathbf{e} \times \mathbf{e}') \cdot F_s(k)$ with $\mathbf{k} = \mathbf{q} - \mathbf{q}'$ where $\mathbf{e}$ and $\mathbf{q}$ ($\mathbf{e}'$ and $\mathbf{q}'$) are, respectively, the polarization vector and wave-vector of the primary (secondary) photon, and the Bragg angle θ that appears in structure factors for resonant scattering is defined by $\mathbf{q} \cdot \mathbf{q}' = q^2 cos(2\theta)$. $F_s(k)$ is the unit-cell structure factor for spin magnetic moments. The measured energy profiles of reflections $(0,0,3)_h$ and $(0,0,9)_h$ show a single resonance in the pre-edge region, devoid of secondary structure, which is modelled by a single oscillator centred at an energy $\Delta = 7.105$ keV with a width Γ, to an excellent approximation.[7] In this instance, the resonant contribution to scattering is represented by $d(E)F_{\mu'\nu}$ where $d(E) = \Delta/[E - \Delta + i\Gamma]$ and $F_{\mu'\nu}$ is a unit-cell structure factor for states of polarization μ'(secondary) and ν (primary). We follow the standard convention for orthogonal polarization labels σ and π; σ normal to the plane of scattering and, consequently, π in the plane. Unit-cell structure factors listed in an Appendix are derived following steps for the corundum structure found in Lovesey et $al.$[19] The generic form of our Bragg scattering amplitude for haematite at a space-group forbidden reflection (no Thomson scattering) is,

$$G_{\mu'\nu}(E) = G^s_{\mu'\nu} + \rho \, d(E) \, F_{\mu'\nu}, \tag{1}$$

where ρ is a collection of factors, which include radial integrals for particular resonance events, that are provided in an Appendix.

Atomic multipoles $\langle T^K_Q \rangle$ in parity-even structure factors, for E1-E1 and E2-E2 events, have the property that even rank K are time-even (charge) and odd rank K are time-odd (magnetic). For enhancement at the K-absorption edge, all parity-even atomic multipoles relate to orbital degrees of freedom in the valence shell - spin degrees of freedom are absent Lovesey.[24] Thus, for enhancement at the K-absorption edge, multipoles $\langle T^K_Q \rangle$ with odd K are zero if the ferric, $3d^5$ (electron configuration ^{6}S) of the iron ion is fully preserved in haematite. The measured iron magnetic moment 4.9 μ_B at 77 K indicates that the orbital magnetic moment is small and likely no more than $\approx 2\%$ of the measured moment.[2,5]

III. PHASE I

We report first our analyses of data gathered by Kokubun *et al.*[7] on haematite at 150 K. With 100% incident σ-polarization and no analysis of polarization in the secondary beam, the measured intensity of a Bragg reflection is proportional to,

$$I = \mid G_{\sigma'\sigma}(E) \mid^2 + \mid G_{\pi'\sigma}(E) \mid^2, \tag{2}$$

For a collinear antiferromagnet, in expression (1) for $G_{\mu'\nu}(E)$ one has $G_{\sigma'\sigma}^s = 0$ and in the channel with rotated polarization,

$$G_{\pi'\sigma}^s = 4\,sin(\theta)\,sin(\varphi l)\,(E/mc^2)\,f_s(k)\,\langle S^z \rangle, \tag{3}$$

where $\varphi = -37.91$ deg., the Bragg angle $\theta = 10.96$ deg. $(34.77\ deg.)$ for a Miller index $l = 3$ (9), $\langle S^z \rangle \le 5/2$ is the spin moment and $f_s(k)$ is the spin form factor with $f_s(0) = 1$. Note that $\mid G_{\pi'\sigma}^s \mid^2 \propto sin^2(\theta)$ above is not the expression in equation (20) in Ref. (7), which is derived by use of an abridged scattering amplitude that is not valid in the experiment.[22]

At resonance, the spin contribution $G_{\pi'\sigma}^s$ is suppressed compared to the resonant contribution by a factor $\Gamma/\Delta \approx 10^{-4}$ and it may safely be neglected.

Confrontations between our theoretical expressions for the azimuthal-angle dependence of Bragg intensity with corresponding experimental data reported in Ref. (7) reveal a 30 deg. mismatch of origins in the azimuthal angle. Our origin $\psi = 0$ has the a-axis normal to the plane of scattering[19] whereas Kokubun *et al.*[7] specify an origin such that the a-axis is parallel to $\mathbf{q} + \mathbf{q}'$ giving a nominal mismatch in the origin of ψ, between theory and experiment, of 90 deg. The actual mismatch, 30 deg., revealed by our analysis of data is likely to arise in the experiments by mistakenly using for reference a basal plane Bragg reflection off-set by 60 deg. In this and the following section we reproduce data as a function of ψ off-set by 30 deg. compared to data reported in Figures 5 and 10 in Ref. (7).

In light of the established negligible orbital magnetism in haematite, parity-even, time-odd atomic multipoles ($K = 1\,\&\,3$) are set equal to zero. Looking in the Appendix one finds $F_{\mu'\nu}(E1 - E1) = 0$. Additionally, $F_{\sigma'\sigma}(E2 - E2) = 0$ and $F_{\pi'\sigma}(E2 - E2)$ produces Templeton - Templeton scattering proportional to $[\langle T_{+3}^4 \rangle' cos(3\psi)]$, where ψ is the azimuthal angle. Inspection of data for phase I reproduced in figure 2 shows that an E2-E2 event on its own is not an adequate representation. The missing modulation is produced by the E1-E2 event that introduces a polar quadrupole $\langle U_0^2 \rangle$ in phase with the parity-even hexadecapole.[25] Figure 2 displays satisfactory fits of $\{\mid F_{\sigma'\sigma} \mid^2 + \mid F_{\pi'\sigma} \mid^2\}$, using equal measures of E1-E2 and E2-E2 events, to data from azimuthal-angle scans performed at reflections $(0, 0, l)_h$ with $l = 3$ and 9. The influence of the polar quadrupole is very notable for $l = 9$ because for this Miller index the hexadecapole is suppressed, with the ratio at $l = 9$ to $l = 3$ of $tan(\varphi l)$ equal to 0.15. Relative values of multipoles inferred from fits to the low temperature data are gathered in table I. Values of $\langle T_{+3}^4 \rangle'$ and $\langle U_0^2 \rangle$ in phase I are found to be of one sign and in the ratio 20 : 1, with near equal magnitudes of the polar quadrupole and magneto-electric octupole, $\langle G_{+3}^3 \rangle'$. If $\mid \rho(E2 - E2)/\rho(E1 - E2) \mid \approx 1.0$, as suggested by our estimate, magneto-electric multipoles are $\approx 5\%$ of the dominant parity-even hexadecapole, $\langle T_{+3}^4 \rangle'$.

Without polarization analysis, it does not seem possible from azimuthal-angle scans to distinguish between E1-E2 and E2-E2 events. However, as shown in Section 5, the two events can be distinguished with circularly polarized x-rays.

The failure of pure parity-even structure factors E1-E1 plus E2-E2 to explain the data is most pronounced for $l = 9$. To illustrate the extent of the failure, figure 3 displays a fit to intensity at $l = 9$ with an amplitude made of equal amounts of E1-E1 and E2-E2 unit-cell structure factors, and the quality of the fit is clearly inferior to the one shown in figure 2.

IV. PHASE II

In this phase, above the Morin transition, iron magnetic moments lie in a plane normal to the c-axis. We choose orthonormal principal-axes (x, y, z) with the x- and z-axes parallel to the crystal a- and c-axes, respectively. The crystal a-axis is parallel to a diad axis of rotation symmetry, normal to the mirror plane that contains the trigonal c-axis.

The spin contribution $G_{\sigma'\sigma}^s = 0$, while the corresponding $\pi'\sigma$-scattering amplitude can be different from zero and, notably, it depends on azimuthal angle. We find,
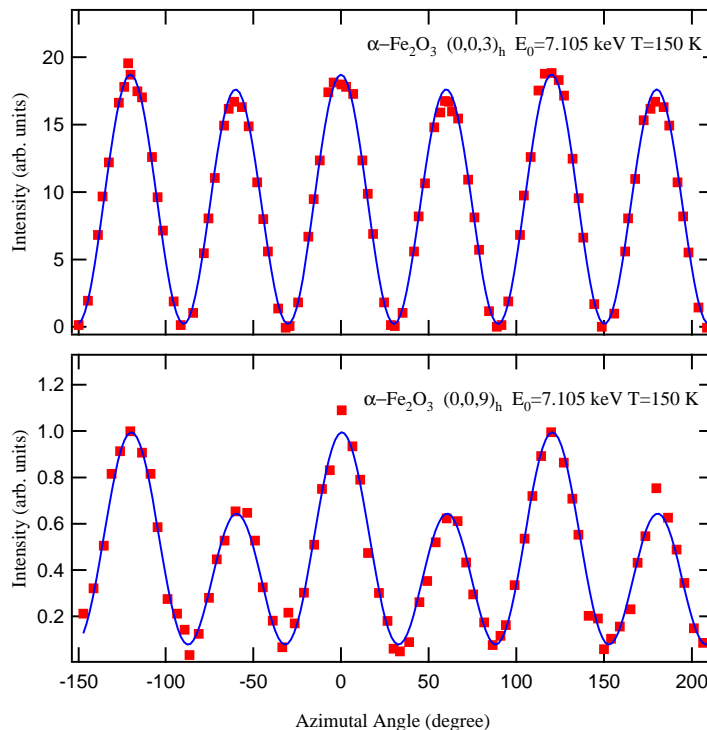
FIG. 2. Azimuthal-angle dependence of intensity of Bragg reflections $(0,0,l)_h$ with $l = 3$ and $l = 9$ for phase I $(150K)$. Continuous curves are fits to structure factors for E1-E2 and E2-E2 events with magnetic (time-odd) parity-even multipoles set to zero. Inferred relative atomic multipoles are listed in Table I. Experimental data is taken from Kokubun et al.[7]

TABLE I. Relative values of atomic multipoles for collinear antiferromagnetism in phase I (at $\approx 100\,\text{K}$ below the Morin transition) and canted antiferromagnetism in phase II (room temperature). The magnitude of the dominant hexadecapole, $\langle T^4_{+3}\rangle'$, is set to $+ 10.00$. The estimate $\langle U^2_0\rangle = +0.50$ inferred by fits to data for phase I is also used in analysis of data for phase II. Values for other multipoles are inferred by fitting to data equal measures of E1-E2 and E2-E2 structure factors listed in an Appendix, with time-odd figures (magnetic) multipoles in E2-E2 set to zero. Fits are displayed in figures 2 and 4.

With our definition, real $\langle...\rangle'$ and imaginary $\langle...\rangle''$ parts of a multipole are defined through $\langle G^K_Q\rangle = \langle G^K_Q\rangle' + i\langle G^K_Q\rangle''$ with $\langle G^K_Q\rangle^* = (-1)^Q\langle G^K_{-Q}\rangle$, and identical relations for the other two multipoles, $\langle T^K_Q\rangle$ and $\langle U^K_Q\rangle$. All multipoles with projection Q = 0 are purely real. Using radial integrals from an atomic code factors in equation (1) are in the ratio $\rho(E2-E2)/\rho(E1-E2) \approx -0.98$, which is no more than a guide to the actual value in haematite. This ratio is not eliminated in listed values of multipoles.

Multipole	Phase I	Phase II
$\langle G^1_{+1}\rangle'$	−	0.50(2)
$\langle G^2_0\rangle$	0.11(2)	−
$\langle G^2_{+1}\rangle''$	−	−0.38(3)
$\langle G^3_{+1}\rangle'$	−	1.07(6)
$\langle G^3_{+3}\rangle'$	0.41(2)	2.45(5)

$$G^s_{\pi'\sigma} = 4\cos(\psi)\cos(\theta)\sin(\varphi l)\,(E/mc^2)\,f_s(k)\,\langle S^y\rangle, \tag{4}$$

and $\mid G^s_{\pi'\sigma}\mid^2 \propto \cos^2(\theta)$ from eq. (4) is not the same as the corresponding result, equation (19) in Ref. (7) for reasons spelled out in Section 3.

Away from a resonance, the result (4) predicts a two-fold periodicity of intensity as a function of azimuthal angle, which is in accord with observations in Ref. (7). Spin moment in the mirror plane $\langle S^y\rangle$ is close to 5/2 while spontaneous magnetization, directed along a diad axis, is $\approx 0.02\%$ of the nominal value. From (3) and (4) we see that the ratio of $\mid G^s_{\pi'\sigma}\mid^2$ for phases I and II depends on $tan^2(\theta)$ which takes the value 0.04(0.48) for $l = 3(l = 9)$. For $l = 3$, Kokubun et al.[7] report intensity between 150 K (phase I) and 300 K (phase II). Starting from ≈ 210 K a large
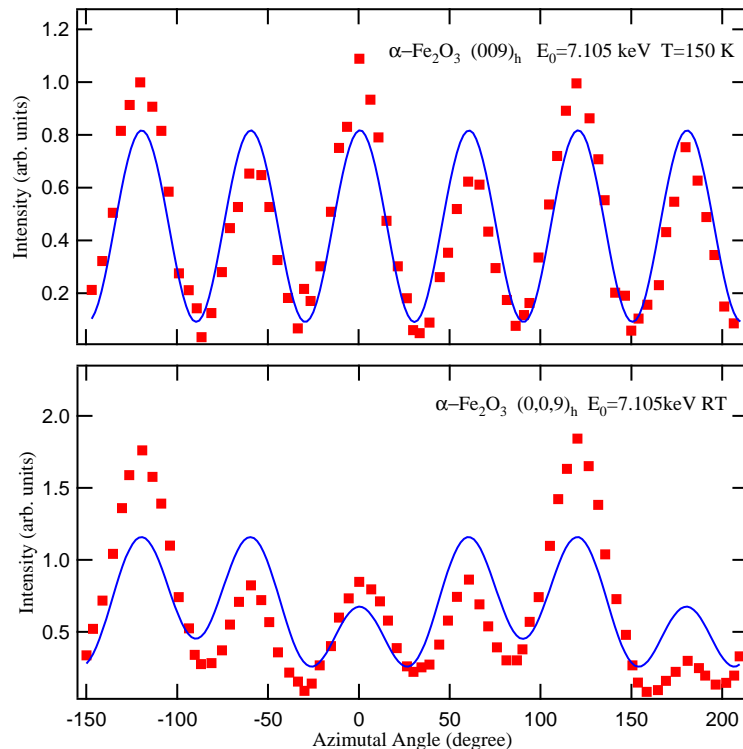
FIG. 3. Azimuthal-angle dependence of intensity of the Bragg reflection $(0, 0, 9)_h$ for phases I $(150K)$ and II (room temperature). Continuous curves are fits to parity-even structure factors E1-E1 and E2-E2 including all magnetic multipoles. Experimental data taken from Kokubun *et al.*[7] appears also in figure 2 and 4.

increase of intensity is observed over an interval of ≈ 40 K. Rotation of magnetic moments from the c-axis to basal plane, between phases I and II, takes place in a range of 10 K in pure crystals but the interval can be larger in mixed materials as commented above.

Slightly away from the resonance, interference between the non-resonant, spin contribution (4) and $d(E)F_{\pi'\sigma}$ may enhance intensity in a Bragg peak if $(E - \Delta)[G^s_{\pi'\sigma}/(F_{\pi'\sigma})'])0$. We find $[G^s_{\pi'\sigma}/(F_{\pi'\sigma})']$ is of one sign for $l = 3$ and $l = 9$ provided that $f_s(k)$, the spin form factor, is of one sign. At face value this finding is not at one with Kokubun *et al.*[7] who discuss a sighting of slight enhancement of the intensity on the low-energy side of the resonance for $l = 9$ that is apparently absent, or completely negligible, for $l = 3$.

Figure 4 shows fits of E1-E2 and E2-E2 structure factors to data gathered at $l = 3$ and $l = 9$ in phase II (room temperature). As before, in our analysis of data gathered on phase I, parity-even multipoles with odd K are set to zero. Time-even contributions to structure factors, determined by chemical structure, are taken to be the same in phases I and II. Consistency with this assumption, about chemical structure, implies for phases I and II the same values of $\langle T^4_{+3}\rangle'$ and $\langle U^2_0\rangle$. Inferred relative values of time-odd atomic multipoles for phase II are listed in Table I, with values of $\langle T^4_{+3}\rangle'$ and $\langle U^2_0\rangle$ in the ratio 20 : 1. Relative to the magnitude of $\langle U^2_0\rangle$, none of the magneto-electric multipoles are negligible in phase II. Figure 3 contains a fit of pure parity-even structure factors, E1-E1 and E2-E2, to data for the reflection l = 9, and the quality of the fit is clearly inferior to that reported in figure 4 with E1-E2 and E2-E2 structure factors.

V. CHIRAL STATE

A chiral, or handed, state of a material is permitted to couple to a probe with a like property, in our case circular polarization (helicity) in the primary beam of x-rays. In our notation, the pseudo-scalar for helicity, P_2, is one of three purely real, time-even Stokes parameters. Intensity induced by helicity in the primary beam is,[17]

$$I_c = P_2 \, Im \, \{G^*_{\sigma'\pi} G_{\sigma'\sigma} + G^*_{\pi'\pi} G_{\pi'\sigma}\}, \tag{5}$$
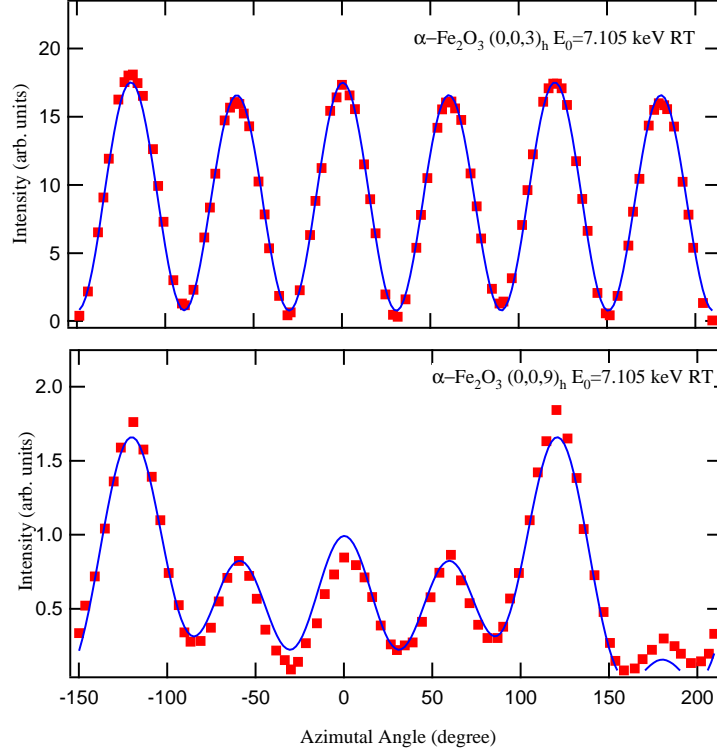
FIG. 4. Azimuthal-angle dependence of intensity of Bragg reflections $(0, 0, l)_h$ with $l = 3$ and $l = 9$ for phase II (room temperature). Continuous curves are fits to structure factors for E1-E2 and E2-E2 events with magnetic (time-odd) parity-even multipoles set to zero. Inferred relative atomic multipoles are listed in Table I. Experimental data is taken from Kokubun et $al.$[7]

where the amplitudes $G_{\mu'\nu}$ are given by eq. (1) and * denotes complex conjugation. I_c is zero for Thomson scattering since it is proportional to $(\mathbf{e} \cdot \mathbf{e}')$ and diagonal with respect to states of polarization.

Let us consider the fully compensating collinear antiferromagnet (phase I). For both E1-E1 and E1-M1 events there are no contributions diagonal with respect to states of polarization and I_c is zero. Using structure factors listed in the Appendix for the E1-E2 and E2-E2 events we find,

$$I_c(E1 - E2) = -P_2 \left(\frac{8\sqrt{2}}{5}\right)\rho^2(E1 - E2) \mid d(E) \mid^2 sin(3\psi) cos^3(\theta) (1 + sin^2(\theta))cos^2(\varphi l)\langle G_{+3}^3\rangle'\langle U_0^2\rangle, \qquad (6)$$

and,

$$I_c(E2 - E2) = -P_2 \, 4\rho^2(E2 - E2) \mid d(E) \mid^2 \; sin(6\psi)sin(\theta) cos^6(\theta) sin^2(\varphi l)\langle T_{+3}^3\rangle''\langle T_{+3}^4\rangle', \qquad (7)$$

The predicted intensities are significantly different - notably in dependence on the azimuthal angle - and offer a method by which to distinguish contributions from the two events. Intensities (6) and (7) depend on long-range magnetic order, with $I_c(E2 - E2) = 0$ if the ferric ion is pure ^{6}S. The polar quadrupole in (6) is a manifestation of local chirality[19,25] whereas the pseudoscalar $\langle U_0^0\rangle$, discussed in the next section, is a conventional measure of the chirality of a material. While for phase II, we find that Ic is given by,

$$I_c(E1 - E2) = P_2 \left(\frac{8\sqrt{2}}{5}\right) \rho^2(E1 - E2) \mid d(E) \mid^2 \; cos^2(\varphi l) cos^2(\theta) \langle U_0^2\rangle \{ \frac{1}{\sqrt{3}} sin(\psi) \, [\frac{-3}{\sqrt{5}} (cos(3\theta) + cos(\theta)) \langle G_{+1}^1\rangle' +$$

$$+(cos(3\theta) - cos(\theta)) \langle G_{+1}^2\rangle'' - \frac{1}{\sqrt{5}} (cos^3(\theta) + 2cos(\theta)) \langle G_{+1}^3\rangle'] - sin(3\psi) cos(\theta) (1 + sin^2(\theta))\langle G_{+3}^3\rangle'\},$$
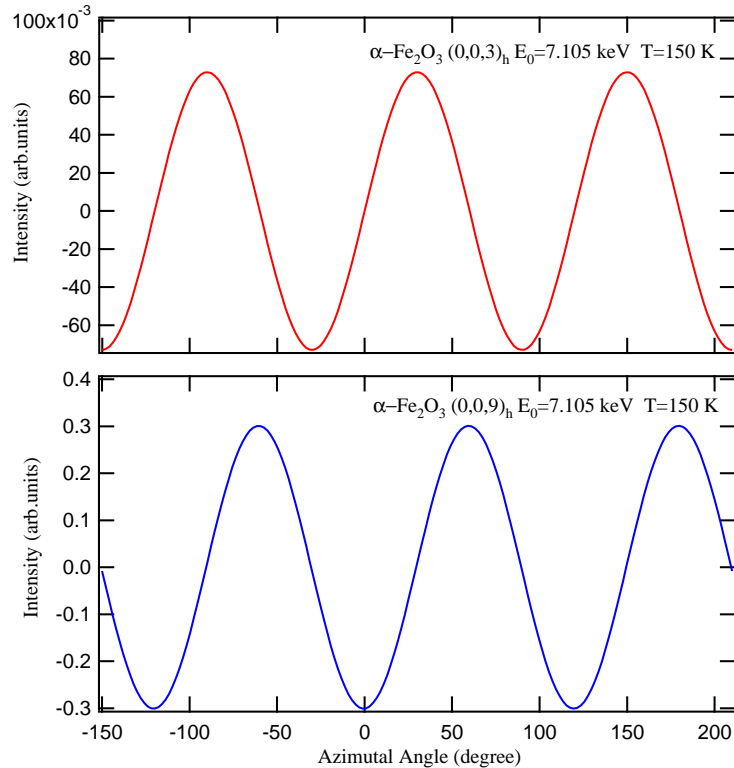
$$(8)$$

FIG. 5. Simulation of the azimuthal-angle dependence from eq. (6) for a circular polarized light of Bragg reflections $(0, 0, l)_h$ with $l = 3$ and $l = 9$ for Phase I. Continuous curves are simulations made with the values of the multipoles from the E1-E2 event gathered in Table I. For the E2-E2 event I_c is zero because our magnetic (time-odd) parity-even multipoles are zero for a ferric ion. Zero I_c does not mean zero intensity for Ic is only the circular polarization contribution to intensity.[17]

$$I_c(E2 - E2) = -P_2(\frac{1}{\sqrt{2}})\,\rho^2(E2 - E2)\mid d(E)\mid^2\,sin^2(\varphi l)\,\langle T^4_{+3}\rangle'\{4\,sin(\psi)\,cos^4(\theta)\,[\frac{-1}{\sqrt{5}}\,sin(\theta)\,(8cos^2(\theta) - 5)\langle T^1_1\rangle'' +$$

$$+\sqrt{\frac{3}{5}}\,sin(\theta)cos^3(\theta)\langle T^3_{+1}\rangle''] - 4\sqrt{2}\,sin(\theta)\,cos^6(\theta)\,sin(6\psi)\,\langle T^3_{+3}\rangle''\},$$

$$(9)$$

VI. MAGNETIC CHARGE AND CHIRALITY

The pseudo-scalar monopoles $\langle G^0_0\rangle$ and $\langle U^0_0\rangle$ have particularly simple and interesting physical interpretations. Both monopoles are allowed in haematite structure factors for the E1-M1 event, as we see by inspection of relevant expressions in the Appendix. A conventional measure of the chirality of electrons in a molecule or extended media is $\langle \mathbf{S} \cdot \mathbf{p}\rangle\,/\mid\langle \mathbf{p}\rangle\mid$, where $\mathbf{S}$ and $\mathbf{p}$ are operators for spin and linear momentum, and, not unsurprisingly, $\langle U^0_0\rangle$ is proportional to $\langle \mathbf{S} \cdot \mathbf{p}\rangle/\mid \mathbf{p}\mid$. It is well-known that, $\langle U^0_0\rangle$ contributes to natural circular dichroism.[26] On the other hand, $\langle G^0_0\rangle$, a magnetic charge, does not contribute to dichroic signals but it can contribute in scattering. Such is the case for gallium ferrate,[27] and phase I of haematite. Magnetic charge, and the magneto-electric quadrupole, are present in the amplitude for back-scattering with $\mathbf{q} = -\mathbf{q}'$.

VII. DISCUSSION

We report successful analyses of resonant Bragg diffraction data gathered by Kokubun *et al.*[7] on haematite in the collinear (phase I) and canted (phase II) antiferromagnetic phases, with no analysis of diffraction according to
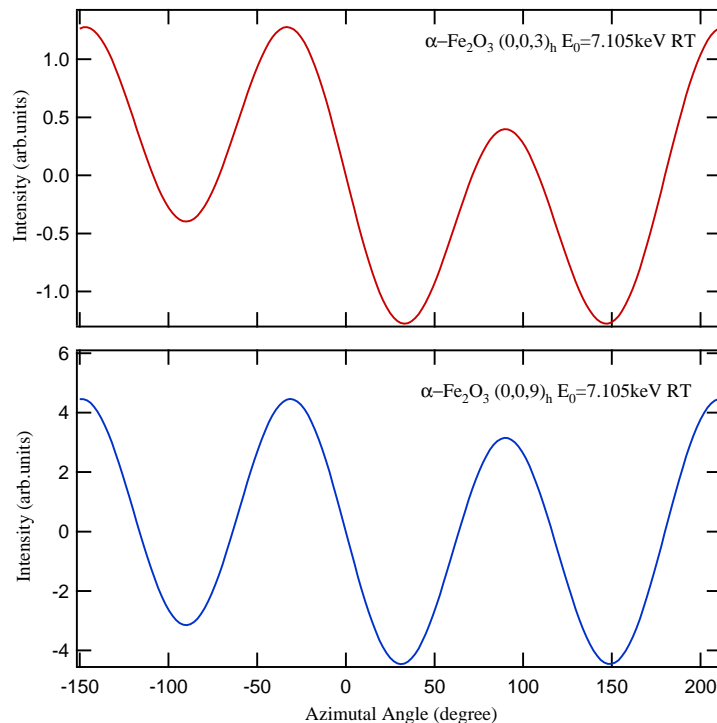
FIG. 6. Simulation of the azimuthal-angle dependence from eq. (8) for a circular polarized light of Bragg reflections $(0, 0, l)_h$ with $l = 3$ and $l = 9$ for Phase II (room temperature). Continuous curves are simulations made with the values of the multipoles from the E1-E2 event gathered in Table I. For the E2-E2 event the Ic is equal to zero because our magnetic (time-odd) parity-even are zero. Zero I_c does not mean zero intensity since I_c is only the circular polarization contribution.[17]

polarization of the x-rays. We infer good estimates of iron atomic multipoles, and find large amounts of parity-odd multipoles. Of particular importance to a successful analysis is a polar quadrupole, a measure of local chirality,[25] and, in phase II, magneto-electric multipoles that include the anapole. Slight departures between our theory and experiment could be due to a less than ideal crystal, as witnessed in the extended interval of temperature for rotation of magnetic moments between phases I and II.[7]

Future experiments might employ polarization analysis that will allow closer scrutiny of unit-cell structure factors for haematite we list in an Appendix, which are derived from the established chemical and magnetic structures of haematite. We predict for phase I that scattering enhanced by the E1-M1 event contains monopoles that represent chirality and magnetic charge.

Our analyses of data are based on an atomic theory of x-ray Bragg diffraction[19] with unit-cell structure factors that are fundamentally different from corresponding structure factors employed by Kokubun *et al.*[7] One difference arises in the treatment of non-resonant magnetic scattering. We use the exact expression, due solely to spin moments, while Kokubun *et al.*[7] mistakenly - because it is not valid in the investigated interval of energy - use an abridged amplitude by de Bergevin and Brunel[22] that is a sum of the exact expression and the high-energy limit of two contributions to scattering that involve intermediate states (one of the two is capable of showing a resonance).Treating the resonance as a single oscillator, in accord with the reported energy profile, our structure factors for resonant diffraction are completely determined with no arbitrary phase factors, unlike the analysis in Ref. (7). This difference in the analyses is a likely explanation of our evidence that published data for azimuthal-angle scans are miss-set by 30 deg. Our treatment of magnetic (time-odd) contributions to scattering is another major difference in the analyses. Whereas Kokubun *et al.*[7] allow only the dipole in the E1-E1 event we consider all permitted time-odd contributions in both parity-even and parity-odd events. Time-odd multipoles from parity-even events, $\langle T_Q^K \rangle$ with odd K, are related to orbital magnetism when the intermediate state in resonance is an s-state, as is the case in the experiments in question with absorption at the iron K-edge. The available evidence is that orbital magnetism of the ferric ion in haematite is negligible, as expected for an s-state ion, and the same can be said of the parity-even, time-odd multipoles, including the dipole which at resonance is the only source of magnetic scattering considered in Ref. (7). From our analysis, we conclude that magnetic scattering at resonance is provided by magneto-electric multipoles in an E1-E2 event. We

demonstrate beyond reasonable doubt that, allowing magnetic $\langle T_Q^K \rangle$ different from zero the available data are not consistent with diffraction enhanced by purely parity-even events, E1-E1 and E2-E2.

In summary, we have derived information on the relative magnitude of multipoles for the antiferromagnetic phases of haematite (above and below the Morin Temperature) These estimates are obtained from analyses of experimental azimuthal dependence gathered in resonant x-ray Bragg diffraction at space-group forbidden reflections $(0, 0, 3)_h$ and $(0, 0, 9)_h$. A chiral electron state is proposed from a predicted coupling of resonant intensity to circular polarization in the primary beam. This effect allows differentiating between contributions of the E1-E2 and E2-E2 events. In addition, pseudo-scalar monopoles (chirality and magnetic charge) are present in the E1-M1 amplitude for resonant scattering by haematite below the Morin temperature.

VIII.   ACKNOWLEDGMENTS

Appendix A: Unit-cell structure factors

Some factors in eq.(1) contain a dimensionless quantity $\aleph = m\Delta a_o^2/\hbar^2 = 260.93$ where a_o is the Bohr radius and $\Delta = 7.105 keV$. Radial integrals for the E1 and E2 processes at the K-absorption edge are denoted by $\{R\}_{sp}$ and $\{R^2\}_{sd}$. Estimates from an atomic code are $\{R\}_{1s4p}/a_o = -0.0035$ and $\{R^2\}_{1s3d}/a_o^2 = 0.00095$, and it is interesting that the magnitudes are smaller than hydrogenic values with $Z = 26$ by a factor of about three. More appropriate values of the radial integrals will be influenced by ligand ions. The M1 process between stationary states of an isolated non-relativistic ion is forbidden because the radial overlap of initial and final states in the process is zero, on account of orthogonality. For an M1 process in a compound the radial integral, denoted here by $\{1\}_{\gamma\gamma}$, is an overlap of two orbitals with common orbital angular momentum, Γ, which may be centred on different ions. The magnitude of $\{1\}_{\gamma\gamma}$ is essentially a measure of configuration interactions and bonding, or covalancy, of a cation and ligands. Factors appearing in eq.(1) are,

$$\rho(E1 - E1) = [\{R\}_{sp}/a_o]^2 \aleph, \tag{A1}$$

$$\rho(E1 - M1) = q\{R\}_{sp}\{1\}_{\gamma\gamma}, \tag{A2}$$

$$\rho(E1 - E2) = [q\{R^2\}_{sd}R_{sp}/a_o^2]\aleph, \tag{A3}$$

$$\rho(E2 - E2) = [q\{R^2\}_{sd}/a_o]^2 \aleph. \tag{A4}$$

Haematite structure factors $F_{\mu'\nu}$ for forbidden reflections $(0, 0, l)_h$ with $l = 3(2n + 1)$ and enhancements by E1-E1, E1-M1, E1-E2 and E2-E2 events are listed below. In these expressions, the angle $\varphi = -\pi u$, where $u = 2z - 1/2 = 0.2104$ for $\alpha - Fe_2O_3$, the angle θ is the Bragg angle, and $\langle T_Q^K \rangle$, $\langle G_Q^K \rangle$ and $\langle U_Q^K \rangle$ are the mean values of the atomic tensors involved.

1.   Collinear antiferromagnet, phase I

(E1-E1)

$$F_{\sigma'\sigma}(E1 - E1) = 0 \tag{A5}$$

$$F_{\pi'\sigma}(E1 - E1) = -2\sqrt{2}sin(\varphi l)sin(\theta)\langle T_0^1\rangle \tag{A6}$$

$$F_{\pi'\pi}(E1 - E1) = 0 \tag{A7}$$

(E1-M1)

$$F_{\sigma'\sigma}(E1 - M1) = 0 \tag{A8}$$

$$F_{\pi'\sigma}(E1 - M1) = \frac{2\sqrt{2}}{\sqrt{3}}cos(\varphi l)\{2\sqrt{2}[-sin^2(\theta)\langle G_0^0\rangle + icos^2(\theta)\langle U_0^0\rangle] + (2 + cos^2(\theta))\langle G_0^2\rangle + icos^2(\theta)\langle U_0^2\rangle\} \tag{A9}$$

$$F_{\pi'\pi}(E1 - M1) = 0 \tag{A10}$$

(E1-E2)

$$F_{\sigma'\sigma}(E1 - E2) = -\frac{4\sqrt{2}}{\sqrt{5}}sin(3\psi)cos(\varphi l)cos(\theta)\langle G_{+3}^3\rangle' \tag{A11}$$

$$F_{\pi'\sigma}(E1 - E2) = \frac{2}{\sqrt{5}}cos(\varphi l)\{-[3cos^2(\theta) - 2]\langle G_0^2\rangle + icos^2(\theta)\langle U_0^2\rangle + \sqrt{2}sin(2\theta)cos(3\psi)\langle G_{+3}^3\rangle'\} \tag{A12}$$

$$F_{\pi'\pi}(E1 - E2) = -\frac{4\sqrt{2}}{\sqrt{5}}sin(3\psi)cos(\varphi l)cos(\theta)sin^2(\theta)\langle G_{+3}^3\rangle' \tag{A13}$$

(E2-E2)

$$F_{\sigma'\sigma}(E2 - E2) = -\sqrt{2}sin(3\psi)sin(\varphi l)\langle T_{+3}^3\rangle'' \tag{A14}$$

$$F_{\pi'\sigma}(E2 - E2) = \sqrt{\frac{2}{5}}sin(\varphi l)\{sin(3\theta)\langle T_0^1\rangle - sin(\theta)[3cos^2(\theta) - 2]\langle T_0^3\rangle -$$

$$-\frac{\sqrt{5}}{4}cos(3\psi)[[3cos(3\theta) + cos(\theta)]\langle T_{+3}^3\rangle'' - i[cos(3\theta) + 3cos(\theta)]\langle T_{+3}^4\rangle']\} \tag{A15}$$

$$F_{\pi'\pi}(E2 - E2) = -\frac{1}{\sqrt{2}}sin(3\psi)sin(\varphi l)sin(4\theta)\langle T_{+3}^3\rangle'' \tag{A16}$$

2. Canted antiferromagnet, phase II

Time-even contributions to structure factors, determined by chemical structure, are the same in phases I and II. Thus the structure factor with polar multipoles, $F_{\mu'\nu}(u)$, for phase II is identical to the foregoing expression for phase I. With the convenience of the reader in mind, structure factors for parity-even multipoles, $F_{\mu'\nu}(t)$, are given in full although contributions only with K = 1 and 3 differ from foregoing expressions.

(E1-E1)

$$F_{\sigma'\sigma}(E1 - E1) = 0 \tag{A17}$$

$$F_{\pi'\sigma}(E1 - E1) = 4cos(\psi)sin(\varphi l)cos(\theta)\langle T_{+1}^1\rangle'' \tag{A18}$$

$$F_{\pi'\pi}(E1 - E1) = 4sin(\psi)sin(\varphi l)sin(2\theta)\langle T_{+1}^1\rangle'' \tag{A19}$$

(E1-M1)

$$F_{\sigma'\sigma}(E1 - M1) = 8sin(\psi)cos(\varphi l)cos(\theta[-\langle G^1_{+1}\rangle' + \langle G^2_{+1}\rangle''] \tag{A20}$$

$$F_{\pi'\sigma}(E1 - M1) = 4cos(\psi)cos(\varphi l)sin(2\theta)[\langle G^1_{+1}\rangle'] \tag{A21}$$

$$F_{\pi'\pi}(E1 - M1) = -8sin(\psi)cos(\varphi l)cos(\theta)[\langle G^1_{+1}\rangle' + \langle G^2_{+1}\rangle''] \tag{A22}$$

(E1-E2)

$$F_{\sigma'\sigma}(E1 - E2) = \frac{4\sqrt{2}}{\sqrt{5}}cos(\varphi l)cos(\theta) \left\{ \frac{1}{\sqrt{3}}sin(\psi)[\frac{-3}{\sqrt{5}}\langle G^1_{+1}\rangle' - \langle G^2_{+1}\rangle'' + \frac{1}{\sqrt{5}}\langle G^3_{+1}\rangle'] - sin(3\psi)\langle G^3_{+3}\rangle'\right\} \tag{A23}$$

$$F_{\pi'\sigma}(E1 - E2) = 2\sqrt{\frac{2}{5}}cos(\varphi l)sin(2\theta)\{\frac{cos(\psi)}{\sqrt{3}}[\frac{3}{\sqrt{5}}\langle G^1_{+1}\rangle' - 2\langle G^2_{+1}\rangle'' - \frac{1}{\sqrt{5}}\langle G^3_{+1}\rangle'] - cos(3\psi)\langle G^3_{+3}\rangle'\} \tag{A24}$$

$$F_{\pi'\pi}(E1 - E2) = -\frac{4\sqrt{6}}{5}cos(\varphi l)\{\sqrt{\frac{5}{3}}cos(\theta)sin^2(\theta)sin(3\psi)\langle G^3_{+3}\rangle' +$$
$$+sin(\psi)[cos(3\theta)[\langle G^1_{+1}\rangle' - \frac{\sqrt{5}}{3}\langle G^2_{+1}\rangle''] + \frac{1}{3}[cos^3(\theta) + 3cos(\theta)]\langle G^3_{+1}\rangle']\} \tag{A25}$$

(E2-E2)

$$F_{\sigma'\sigma}(E2 - E2) = sin(2\theta)sin(\varphi l)\{sin(\psi)[\frac{-2}{\sqrt{5}}\langle T^1_{+1}\rangle'' - \sqrt{\frac{6}{5}}\langle T^3_{+1}\rangle''] + \sqrt{2}sin(3\psi)\langle T^3_{+3}\rangle''\} \tag{A26}$$

$$F_{\pi'\sigma}(E2 - E2) = -sin(\varphi l)\{cos(\psi) \times [\frac{2}{\sqrt{5}}cos(3\theta)\langle T^1_{+1}\rangle'' + \sqrt{\frac{6}{5}}cos(\theta)(1 + sin^2(\theta))\langle T^3_{+1}\rangle''] +$$
$$+cos(3\psi)[\sqrt{2}cos(\theta)(3cos^2(\theta) - 2)\langle T^3_{+3}\rangle'']\} \tag{A27}$$

$$F_{\pi'\pi}(E2 - E2) = \frac{1}{\sqrt{2}}sin(\varphi l)sin(4\theta)\{sin(\psi)[-\frac{4\sqrt{2}}{\sqrt{5}}\langle T^1_{+1}\rangle'' + \sqrt{\frac{3}{5}}\langle T^3_{+1}\rangle''] - sin(3\psi)\langle T^3_{+3}\rangle''\} \tag{A28}$$

[1] A. H. Morrish, *Canted Antiferromagnetism: Hematite* (World Scientific Publishing, Singapore, 1994).

[2] M. Catti, G. Valerio, and R. Dovesi, Phys. Rev. B **51**, 7441 (1995).

[3] I. Dzyaloshinsky, J. Phys. Chem. Solids **4**, 241 (1958).

[4] T. Moriya, Phys. Rev. **120**, 91 (1960).

[5] E. Krén, P. Szabó, and G. Konczos, Phys. Lett. **19**, 103 (1965).

[6] K. D. Finkelstein, Q. Shen, and S. Shastri, Phys. Rev. Lett. **69**, 1612 (1992).

[7] J. Kokubun, A. Watanabe, M. Uehara, Y. Ninomiya, H. Sawai, N. Momozawa, K. Ishida, and V. E. Dmitrienko, Phys. Rev. B **78**, 115112 (2008).

[8] D. Templeton and L. Templeton, Acta Crystallogr., Sect. A: Cryst. Phys., Diffr., Theor. Gen. Crystallogr. **38**, 62 (1982).

[9] S. W. Lovesey and V. Scagnoli, J. Phys.: Condens. Matter **21**, 474214 (2009).

[10] J. Fernández-Rodríguez, J. A. Blanco, P. J. Brown, K. Katsumata, A. Kikkawa, F. Iga, and S. Michimura, Phys. Rev. B **72**, 052407 (2005).

[11] S. W. Lovesey, J. Fernández-Rodríguez, J. A. Blanco, D. S. Sivia, K. S. Knight, and L. Paolasini, Phys. Rev. B **75**, 014409 (2007).

[12] J. Fernández-Rodríguez, V. Scagnoli, C. Mazzoli, F. Fabrizi, S. W. Lovesey, J. A. Blanco, D. S. Sivia, K. S. Knight, F. de Bergevin, and L. Paolasini, Phys. Rev. B **81**, 085107 (2010).

[13] S. B. Wilkins, R. Caciuffo, C. Detlefs, J. Rebizant, E. Colineau, F. Wastin, and G. H. Lander, Phys. Rev. B **73**, 060406 (2006).

[14] J. A. Paixão, C. Detlefs, M. J. Longfield, R. Caciuffo, P. Santini, N. Bernhoeft, J. Rebizant, and G. H. Lander, Phys. Rev. Lett. **89**, 187202 (2002).

[15] S. W. Lovesey and K. S. Knight, J. Phys.: Condens. Matter **12**, 2367 (2000).

[16] Y. Tanaka, T. Inami, S.W. Lovesey, K.S. Knight, F. Yakhou, D. Mannix, J. Kokubun, M. Kanazawa, K. Ishida, S. Nanao, T. Nakamura, H. Yamauchi, H. Onodera, K. Ohoyama, and Y. Yamaguchi, Phys. Rev. B **69**, 024417 (2004).

[17] J. Fernández-Rodríguez, S. W. Lovesey, and J. A. Blanco, Phys. Rev. B **77**, 094441 (2008).

[18] S. W. Lovesey and K. S. Knight, J. Phys.: Condens. Matter **12**, L367 (2000).

[19] S. W. Lovesey, E. Balcar v K. S. Knight, and J. Fernández-Rodríguez, Phys. Rep. **411**, 233 (2005).

[20] S. W. Lovesey and E. Balcar, J. Phys. Soc. Jpn. **79**, 074707 (2010).

[21] S. W. Lovesey and E. Balcar, J. Phys. Soc. Jpn. **79**, 104702 (2010).

[22] F. De Bergevin and M. Brunel, Acta Crystallogr. A **37**, 324 (1981).

[23] S. W. Lovesey, Rep. Prog. Phys. **56**, 257 (1993).

[24] S. W. Lovesey, J. Phys.: Condens. Matter **10**, 2505 (1998).

[25] V. E. Dmitrienko and E. N. Ovchinnikova, Acta Crystallogr. A **57**, 642 (2001).

[26] S. P. Collins, S. W. Lovesey, and E. Balcar, J. Phys.: Condens. Matter **19**, 213201 (2005).

[27] U. Staub, Y. Bodenthin, C. Piamonteze, M. García-Fernández, V. Scagnoli, M. Garganourakis, S. Koohpayeh, D. Fort, and S. W. Lovesey, Phys. Rev. B **80**, 140410 (2009).